# Assessing the impact of climate change to landslides at Vejle Denmark, using public data

Kristian Svennevig[1], Julian Koch[1], Marie Keiding[1], Gregor Luetzenburg[1,2]

[1] Geological Survey of Denmark and Greenland, GEUS, Copenhagen, Denmark

5    [2] Department of Geosciences and Natural Resource Management, University of Copenhagen, Copenhagen, Denmark

*Correspondence to Kristian Svennevig (ksv@geus.dk)*

**Abstract**

The possibility of increased landslide activity as a result of climate change has often been suggested, but few studies 10   quantify this connection. Here, we present and utilize a workflow for the first time using solely publicly available data to assess the impact of future changes in landslide dynamic conditioning factors on landslide movement. In our case we apply the workflow to three slow-moving coastal landslides at Vejle, presenting the first study of its kind on Danish landslides. We examine modelled Water Table Depth (WTD) as a dynamic conditioning factor using the DK-HIP-model (Danish Hydrology Information and Prognosis system) that simulates historic and future WTD. The 15   data shows a clear correlation with landslide movement as recorded by Interferometric Synthetic-Aperture Radar (InSAR) time series, for the period 2015 to 2019. Movement of up to 84 mm/y occurs during wet winter months when normalized WTD exceeds +0.5 m. During dry winters no, or very little, seasonal landslide movement is observed. The DK-HIP-model predicts an increase of up to 0.7 m in WTD at the study area by 2100 AD under the RCP8.5 scenario (95% confidence) which exceeds the levels this area has experienced in recent decades (mean 20   increase of 0.2 m with standard deviation of 0.25 m). This is likely to result in increased landslide activity and acceleration of movement. In a previous episode of increased landslide activity linked to extreme precipitation in the early 1980'ies, one of the examined landslides accelerated, causing damage to infrastructure and buildings. Our study clearly shows that these landslides are sensitive to climate change and furthermore highlights the potential of utilizing high-quality, publicly available data to address these complex scientific questions. The quality and quantity 25   of such data is ever increasing and so is the potential of this kind of approach.

## 1 Introduction

Landslides can have devastating impacts on infrastructure and human lives in areas with pronounced topography (Froude and Petley, 2018; Mateos et al., 2020). To mitigate these consequences, it is crucial to understand the temporal occurrence and (re-)activation of landslide movement (Pollock and Wartman, 2020). Some studies have 30   shown an increase in landslide activitys as a consequence of climate change (Gariano and Guzzetti, 2016; Crozier, 2010) while others show a reduced activity (Malet et al., 2005; Coe, 2012; Zieher et al., 2023). However, the topic has never been studied in Denmark and never using solely publicly available data.

Conditioning factors for landslides can be divided into static conditioning factors: those that do not change in time, such as lithology and the structural setting, and dynamic conditioning factors; those that change the stability of the slope (preparing factors) and control the timing (triggering factors) of slope failures (Hermanns et al., 2006). Long time series of fluctuations in dynamic conditioning factors, coupled with data on landslide movement, are powerful indicators to examine thresholds in e.g. critical WTD for when slow moving landslides may accelerate. Dynamic conditioning factors may include measured or modeled fluctuations in precipitation (Coe et al., 2004; Kashyap et al., 2021; Handwerger et al., 2022; Dixon and Brook, 2007), water table depth (WTD) (van Asch et al., 2009), permafrost conditions in polar-(Svennevig et al., 2022, 2023) and alpine regions (Magnin et al., 2017, 2019; Penna et al., 2023), snow melt (Moreiras et al., 2012), earthquakes (Saba et al., 2010), landslide toe erosion (Alberti et al., 2022), and changes in land cover (Van Beek and Van Asch, 2004). Movement can be constrained in a number of ways, based both on ground and in-situ measurements (Uhlemann et al., 2016), or remote sensing observations (Scaioni et al., 2014). However, the data used in these studies have often been limited in scope and public availability.

Precipitation can be a dynamic conditioning factor for the (re-)activation of landslides when water infiltrates into the ground and raises the ground water table (Handwerger et al., 2019). A relationship between landslide movements and precipitation/WTD has been observed in several studies where precipitation has been found to be the main factor controlling seasonal activity in deeper slow-moving landslides (van Asch and Buma, 1997; van Asch et al., 1999; Iverson, 2000; Corominas et al., 2005; Handwerger et al., 2019; Luna and Korup, 2022). This is due to rainwater infiltrating the ground and raising the WTD (Iverson, 2000). As a result, the effective normal stress is lowered and the frictional strength of the hillslope is reduced (Terzaghi, 1950). Hydrological drivers of landslide movement are controlled by irregular peak rainfall events and more regular seasonal patterns during wet seasons (Bennett et al., 2016). An increase in temperature due to climate change raises the evapotranspiration, leading to an intensification of the hydrological cycle and a more dynamic shallow water table depth (Collison et al., 2000). Future changes in seasonal precipitation regimes raisng the groundwater table will lead to more frequent attainment of critical water content during rainfall events (Gariano and Guzzetti, 2016). However, it is difficult to constrain general landslide sensitivity to precipitation due to diverse, site-specific conditioning factors (Handwerger et al., 2022).

The amount of publicly available geodata is ever increasing (Vitousek et al., 2023). In recent years, space-born InSAR time series have proven to be a strong tool for covering large areas with high temporal resolution, and the European Ground Motion Service (EGMS) has made such data freely available for most of Europe (Costantini et al., 2022). Moreover, forward modeling of dynamic conditioning factors is increasingly being conducted for local sites (Magnin et al., 2017; Peres and Cancelliere, 2018). Nationwide freely available datasets such as high resolution water table depth modeling are also becoming more widely available (Henriksen et al., 2020).

With this increasing availability of new public data in mind, we set out to answer the question: How will large coastal landslides respond to future climate change? And how far can we get towards answering this question using freely and publicly available data?

70 Compared to many other European countries, relatively little quantitative research has been conducted on landslides in Denmark (Herrera et al., 2018; Mateos et al., 2020; Svennevig and Keiding, 2020; Svennevig et al., 2020). However, a recent study found 3202 landslides in Denmark (Luetzenburg et al., 2022), some of which are in close proximity to developed areas and may pose a threat to infrastructure and livelihoods (Svennevig et al., 2020). One such area is at Mørkholt, a site in Vejle Municipality in eastern Jutland where three large coastal landslides with

75 houses and infrastructure on top were identified. These landsldies have appropiate InSAR reflectors and are covered by the freely availble national water resources model of Denmark, the DK-model. It is thus a good site to address the above research question.

In this study we for the first time quantify the impact of climate change on landslide activity in danish landslides, focusing on slow-moving coastal landslides in Vejle. We do this applying a novel workflow, utilizing publicly

80 available data to model the dynamic conditioning factor of water table depth (WTD). The research identifies an empirical threshold for landslide movement and this is applied for climate projections for 2071–2100 under different Representative Concentration Pathway (RCP) scenarios. The research advances our understanding of the complex relationship between climate change and landslides and offers insights into future risks for these sites while highligting tha potential of utilizing publicly available data for such analyses.

85 The paper is organized as follows: We first go through the methods and data applied in the paper in section 2 "Data and methods". We then present the results on the movement pattern of the landslides and the climate modelling and the correlation of these in section 3. This is followed by discussions of the implications and limitations in section 4 and the summing up of key finding in the conclusion in section 5.
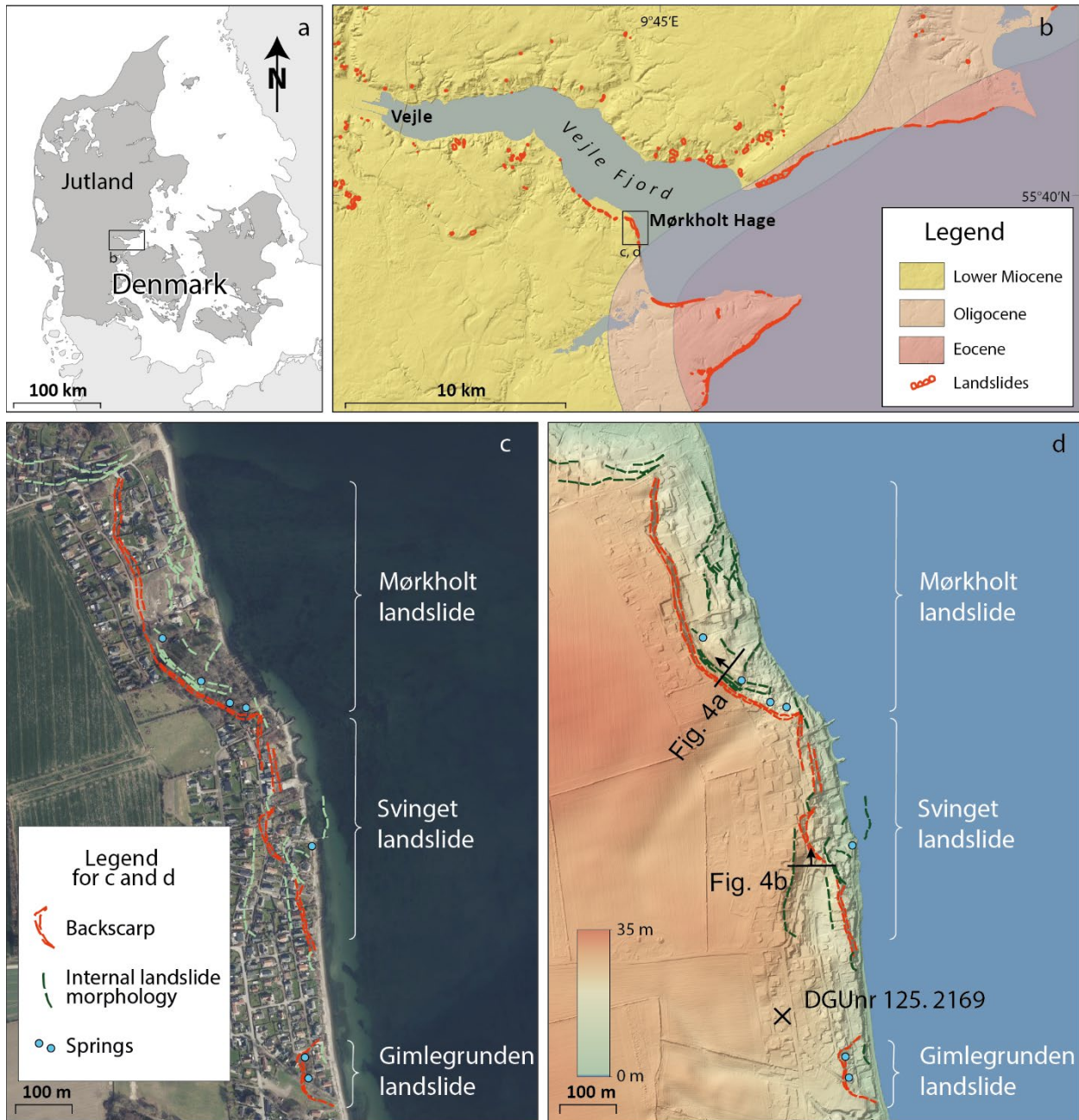
Figure 1. [2 columns] Setting. a) overview map of Denmark showing position of b). b) Regional map of the pre-
quaternary geology *(Håkansson and Pedersen, 1992)* overlain by a shaded Digital Elevation Model (DEM)
(Geodatastyrelsen 2023) and mapped landslides from *(Luetzenburg et al., 2022)* showing position of c) and d). c)
orthophoto from 2021 (Geodatastyrelsen 2023) and d) DEM and hillshade from 2018 of the field area
(Geodatastyrelsen 2023). The dashed line off the coast of the Svinget landslide is a dark lineament on the seabed

*from uplifted black clay. The positions of photos in Fig. 4 are indicated on d) along with the positions of the geothermal well DGUnr 125. 2169 (marked with X).*

### 1.1 Geographic and geological setting

The physiography and near surface geology of Denmark is shaped by several Quaternary glaciations and interglacial periods. The landscape in eastern Jutland consists of sub- and proglacial landforms modified by postglacial fluvial and coastal processes as well as human activity.

The detailed subsurface geology at the Mørkholt field site is poorly known. (Heilmann-Clausen et al., 1985; Rasmussen et al., 2010) describe clays of the Upper Oligocene – Lower Miocene Vejle Fjord Formation from the area. This conforms with the 1:500 000 scale pre-Quaternary bedrock map of Denmark (Håkansson and Pedersen, 1992) indicating the lower part of Miocene at Mørkholt (Fig 1b). In the national drill hole database Jupiter a geothermal well (DGUnr 125. 2169) has been logged in the central part of the field area (Fig 1d). This shows a succession of more than 84 m of marly mudstone, 14 m of black clay topped by 2 m of fine silty sand (Jupiter database drill log, 2023).

Denmark is in the North Temperate Climate Zone and monthly mean temperature ranges between 1°C in January and February and 17°C in July (DMI Weather archive Vejle, 2024).  Mean annual precipitation in Vejle is 766 mm/y which is distributed across the year. Largest rainfall takes typically place in fall and early winter.. Snowfall and snowmelt are sporadic in Denmark and thereby not substantially modulating hydrological processes.

### 1.2 Landslide setting

Three landslides, with combined 47 houses on top, have been mapped on the east facing coastal slope at the Mørkholt field site (Fig. 1c, d): the Mørkholt landslide (27 houses), the Svinget landslide (14 houses) and the Gimlegrunden landslide (six houses). The overall morphological mapping is based on identification of steep (35°–50°) arcuate backscarps in a Digital Elevation Model (DEM) and derived hillshade from 2018 supplemented with mapping of internal morphologies and field validation. Additional landslides are mapped in the areas north-west and south of the three landslides we focus on. These are relict landslides with no indication of recent activity such as smooth morphology and no observed structural damage and deformed trees..

The Mørkholt landslide is the largest of the three sites: 510 m wide (north – south), stretching 130 m inland from the coast, covering 58 000 m² onshore, with an unknown extent into sea. The backscarp is clearly defined by an up to 8 m high arcuate 40° steep inland escarpment. The scarp is highest in the central part and decreases to 5 m to the north and south. The Svinget landslide is morphologically not as well defined as the Mørkholt landslide and a clear single backscarp cannot be identified. The area of the landslide is constrained by a series of 30°–60° steep, up to 6 m high escarpments, which extend 470 m from north to south and reach 90 m inland from the shore. It encompasses an onshore area of 22 000 m². A dark lineament is visible on the seabed 35 m from the shore which could correspond to the toe of the landslide giving it a total width of 125 m. The Gimlegrunden landslide is well defined in the hillshade

130    as a 115 by 55 m arcuate depression in the coastal slope encompassing an onshore area of 6 000 m². It is delimited by an up to 4.5 m high and a 55° sloping backscarp. Based on the descriptions above, we classify the three landslides as rotational clay slides with failure surfaces extending below the adjacent seafloor ("soil slump" *sensu* (Hungr et al., 2014).

## 2 Data and methods

135    The workflow presented in Fig. 2 enables climate forecasting of landslides based on publicly available data summarized in Table 1. The workflow diagram shows all the steps from identification of landslides and assessment of landslide activity (step 1) over analysis of potential thresholds in dynamic conditioning factors (step 2) to climate forecasting of landslide activity (step 3). Step 1 is by now a relatively standard procedure (Herrera et al., 2018;

140    Luetzenburg et al., 2022) while step 2 and 3 applied to open data and applied in Denmark are novel and the focus of this paper. We have used general terms to describe the input data to make the flowchart applicable to cases where other types of displacement data and dynamic conditioning factors are at play. The flowchart is thus intended as a blueprint for the near future when publicly available data applicable for assessing the climatic thresholds for increase in landslide activity will increase in quality and quantity.

145    In step 1A which is the initial step into the workflow the landslide is identified, usually in a DEM or DTM (Svennevig et al., 2020). In step 1B it is determined whether the landslide is active or inactive. This is done badsed on remote displacement data but can also be the objective of an initial field validation. In step 2 time series data of landslide displacement and dynamic preconditioning factors are analysed. In our case this is based on InSAR time series and modelled WTD and precipitation. In step 3 future landslide movement is forecasted by applying

150    forecasted WTD models. This used to examine if future thresholds for landslide stability may be breached.
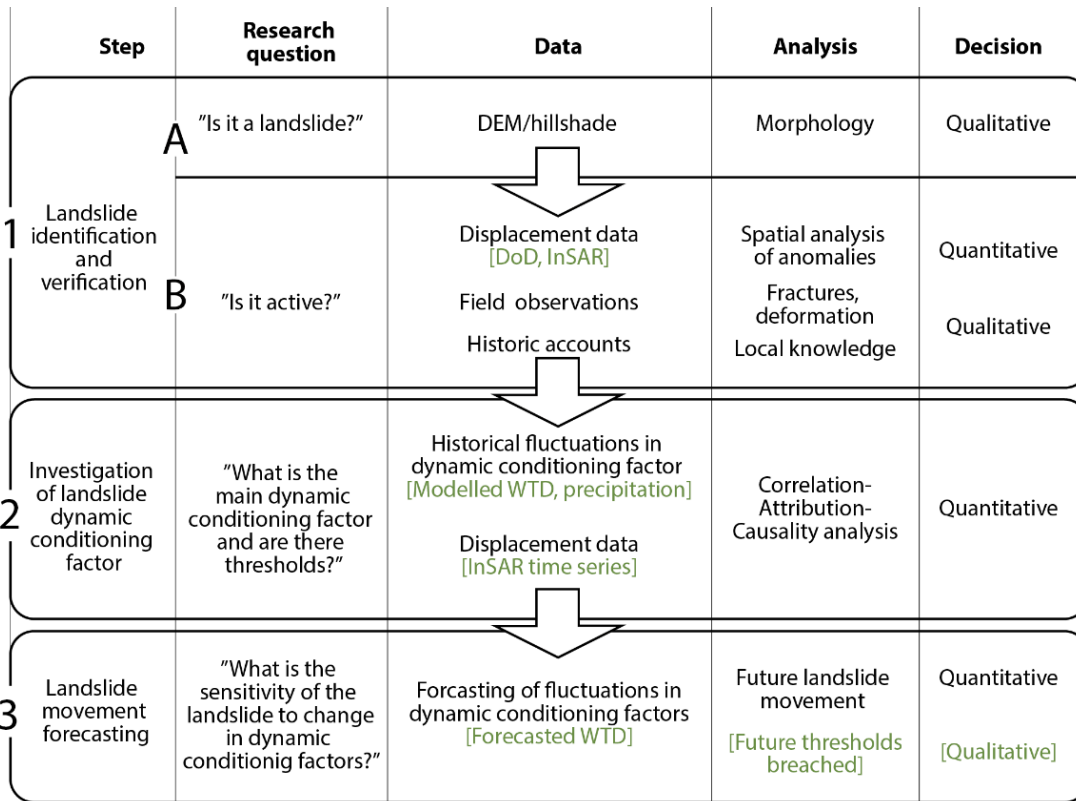
*Figure 2. [two columns] Generalized workflow for identifying landslides and estimating climatic thresholds. The focus of this paper is steps 2 and 3. We have used general terms to describe the input data to make the flowchart applicable to cases where other types of displacement data and dynamic conditioning factors are at play. The specific data used in the present paper is shown in green brackets and in Table 1. DOD stands for Digital Elevation Model of Difference.*

155

| Name/type | Spatial resolution | Temporal resolution | Workflow step (Fig. 2) | Application | Data availability |
|---|---|---|---|---|---|
| SDFI 2014 DEM | 0.4 cm | N/A | 1B | DOD | (SDFI, 2020) |
| SDFI 2018 DEM | 0.4 cm | N/A | 1A | Morphological mapping and DOD | (SDFI, 2020) |
| 2014-2018 DOD | 0.4 cm | 4 years | 1B | Detection of landslide activity: vertical movement | Produced from the above |

| Field observations | N/A | N/A | 1A,B | Field validation | |
|---|---|---|---|---|---|
| Historical accounts | | | 1B,2,3 | Understanding of a potential "worst case" development | |
| EGMS InSAR | N/A | 6 days From 2015 to 2021 | 1B,2 | Movement time series, where reflectors are available | (European Ground Motion Service — Copernicus Land Monitoring Service, 2024) |
| DK-model (HIP – model) | 100 m | Daily hindcast: 1990 to 2019 Daily forecast: 2071-2100 | 2,3 | WTD time series | (Hydrologisk Informations- og Prognosesystem, 2024) |
| DMI Gridded precipitation data | 10 km | Daily sum: 1989 to 2021 | 2 | Precipitation time series | Available through DMI's api. (DMI Weather archive Vejle, 2024) |

*Table 1 overview of data used for this study in the workflow presented in Fig 2.*

160

### 2.1 Lidar DEM and DEM of Difference (DoD)

The Danish Digital Elevation Model (DEM) is provided by the Danish Agency for Data Supply and Infrastructure (SDFI) (Geodatastyrelsen 2023). The dataset is produced from airborne laser (SDFI, 2020). For the area around Mørkholt, the data was acquired in April and May 2018. The product used is delivered with processed to a spatial

165 resolution of 40 cm and with vegetation and buildings removed. The 2018 DEM, and a derived hillshade model, is the basis for the morphological mapping in step 1A of the workflow (Fig. 2) to initially identify the landslides and their extent. This mapping was assisted by orthophotos with a resolution of 12.5 cm also available from SDFI (Luetzenburg et al., 2022).

A nationwide Lidar DEM like the one from 2018 was also produced in 2014 (Table 1). By subtracting the two, a

170 DEM of Difference (DoD) was produced enabling us to evaluate the vertical change in elevation (subsidence, erosion and deposition) between the two acquisitions. Slope parallel transport in the landslides is thus not resolved by this method. It can however be quantified to some degree if the raw laser point files used to produce the DEM's

are used (Pfeiffer et al., 2018), however this is beyond the scope of the present paper. Automatic registering was applied to the two DEM's, to account for minor discrepancies between the two datasets (Nuth and Kääb, 2011). Data was processed in the open source GIS platform QGIS. The result is a 40 cm DoD showing change in elevation down to a vertical accuracy of 1.4 cm between the two acquisition dates. This enables us to effectively detect the spatial extent of vertical changes between the two datasets of down to c. 25 mm/y and thus establish landslide activity in the examined period (step 1B in fig. 2). The spatial resolution is much higher than the Persistent Scatter (PS) point data obtained from InSAR, and the DoD can thus be used to compare whether the InSAR anomalies (PS points showing consistent movement) are indeed representing landslide movement.

## 2.2 InSAR product

Observations of terrain movement are freely available from the European Ground Motion Service (European Ground Motion Service — Copernicus Land Monitoring Service, 2024) (Costantini et al., 2022). The EGMS uses freely available raw data from the Sentinel-1 satellites of the EU Copernicus Earth Observation Program. The satellite emits pulses of radar energy that are scattered and reflected by Earth's surface and recorded back at the satellite. This means that measurements are only obtained where objects at the Earth's surface provide stable reflections of the radar signal, such as bedrock outcrops, houses, and other infrastructure. Vegetated areas or areas with large surface change typically have little or no stable reflectors. Furthermore, very fast or non-linear terrain movements will prevent correlation of the reflected radar signal between acquisitions. In practice for our field area at Mørkholt this means that only houses moving by less than c. 100 mm/y provide good reflectors. The data are provided as PS points and are initially used to screen for a spatial scan for landslide movement in step 1B of the workflow (Fig. 2). In step 2 the time series stored in each individual spatial point is used for a correlation analysis with the dynamic conditioning factor (WTD), see section 2.6. The terrain movements are calculated using Interferometric Synthetic Aperture Radar (InSAR), a technique that uses radar measurements of the Earth's surface from polar orbiting satellites (Crosetto et al., 2016; Rosen et al., 2000; Ferretti et al., 2001; Crosetto et al., 2020). For our study area, at the time of writing, it covers the period from 2015 to 2020. The terrain movements are measured in line-of-sight (LOS) to the satellites; hence the measurements do not provide the absolute vector of movement, but only the part of the movement that projects into the LOS direction. Here, we use data from ascending, i.e., north-going tracks 44 and 117. The ascending satellites look towards ENE, which means that negative movements in LOS indicate movement toward east and down (Fig. 3). By assuming a movement direction of 70°–80° (ENE) and a slope parallel dip of 30°–40°, the LOS records 90%–100% of the actual movement of the landslides. Thus, the ascending satellite geometry is very well suited to study landslide movement at the Mørkholt coast, and we can assume that the movement rates obtained from this method is the actual movement. The movement is reported both as a mean LOS velocity (Fig. 3) and a time series of each InSAR data point (e.g. Fig. 6). In order to reduce the noise of the raw LOS data and to account for the low frequency observations, the time series data are smoothed using a rolling median with a window size of 90 days similar to (Handwerger et al., 2022). This window was chosen because it resulted in a visually satisfying result without any sudden unrealistic uplift caused by noisy data. Data are lacking for

Gimlegrunden and Svinget landslides in the winter 2015/2016 due to an acquisition error observed in all 117A

210    tracks across northern Europe. We have made a linear interpolation across this time period thus providing minimum

movement rates in this period.

**2.3 Field visits and historical accounts**

Field visits were carried out during a two-day inspection in June 2021 to verify remotely sensed observations of the

215    landslide extent and examine potential signs of landslide activity in step 1A and 1B of the workflow (Fig. 2). These

observations are presented in the result section as photos and descriptions of geomorphological expressions of

landslide activity. Accounts from residents and the local history archive have been gathered to constrain an earlier

episode of fast landslide development. These include photos, eyewitness accounts and contemporaneous news items.

220    **2.4 Groundwater modelling**

Modelled (hindcast) Water Table Depth (WTD) is analysed as a potential dynamic conditioning factor for the

landslides by correlation analysis with InSAR movement data (step 2 in Fig. 2). Forecasted WTD is used to examine

the climate sensitivity of the landslide in step 3 of the workflow.

In Denmark, the national water resources model of Denmark, the DK-model, has been continuously developed for

225    the past 25 years by the Geological Survey of Denmark and Greenland (Henriksen et al., 2003; Højberg et al., 2013).

The model represents physically-based descriptions of groundwater flow, surface water dynamics and groundwater-

surface water interactions, integrating water demands for e.g. irrigation and domestic (household) use. The model is

build using the MIKE SHE model code (Abbott et al., 1986) and it is spatially distributed in a 100 m grid. For our

study, we are utilizing the simulation data openly available on  the Danish Hydrological Information and Prognosis

230    system (DK-HIP) (Henriksen et al., 2020). We are primarilaly focusingon simlated water tabel depth (WTD),

defined as the depth below terrain to the uppermost water table  All simulated WTD data presented in this paper are

publicly available via the DK-HIP-model data portal(Hydrologisk Informations- og Prognosesystem, 2024). The

national simulations were subsetted to match the domain of the study area. We have analysed historical and future

simulations. . The historical WTD simulations are at 100 m resolution at daily time step from 1990 to 2019. The data

235    is used to analyse the temporal WTD dynamics for the study area for the period 2015 to 2019, overlapping with the

period of InSAR ground movement. Furthermore, long-term average summer and winter WTD maps at 10 m

resolution (Koch et al., 2021) are used to screen the study site for areas with a distinct WTD seasonality. Climate

change impact simulations for WTD are analysed for Representative Concentration Pathway (RCP)4.5 and RCP8.5

scenarios at 500 m spatial resolution that quantify the changes of WTD for the end of the 21$^{st}$ century. RCP4.5 is the

240    pathway of low to moderate emission throughout the 21$^{st}$ century as defined by IPCC while RCP8.5 is the scenario

of very high future emission towards the year 2100 as defined by IPCC.

The WTD simulations, obtained from the DK-HIP-model data portal, underwent a number of processing steps prior

to the final analysis. A single WTD timeseries at monthly timestep, representing the mean aggregated groundwater

dynamics for the entire study area, has been derived from daily WTD simulation results from 16 selected 100 by 100 m grids (Fig. 5). DK-HIP-model simulations are subject to uncertainty, with a mean error below 1 m for the validation dataset. The model was validated against groundwater head data from a period independent to calibration dataset. The model was not intended to be used at at individual 100 m grids but instead at a more aggregated level to asses catchment scale hydrology. In order to mitigate this, we have first normalize the simulation result by mean division and then aggregate in space and time to obtain a robust timeseries of WTD dynamics for the study area. Simulated WTD can fluctuate and vary sustainably when investigating single grids due to the 3D hydrogeological layer model and boundary conditions which a normalization can take care of. The grids were selected based on two criteria. First, they had to be situated close to the coast in areas collocated with the mapped landslides. Second, the standard deviation of the simulated WTD dynamics may not exceed 2 m, which constrains the analysis to a robust groundwater simulation without drying out of simulation cells resulting in a water table that jumps between computational layers. The first computational layer has a thickness of 2 m and in several cases the WTD jumps from the top layer to deeper computational layers. Further, the 16 WTD timeseries were grid-wise normalized (division by mean) to represent the deviation around mean in order to obtain anomaly timeseries that are comparable with each other. Lastly, the timeseries were aggregated to monthly timescale using the mean function and the monthly variability was calculated by the standard deviation across all grids. The climate change impact was obtained based on simulations at five selected 500 m by 500 m grids (Fig. 5) and the projected change in WTD was calculated as the average across the selected grids on monthly basis. The uncertainty associated to the climate change impact simulations was estimated as the mean climate model ensemble standard deviation. The climate change impact was simulated for both, RCP4.5 and RCP8.5, for a far-future situation representing 2071– 2100. The near future situation representing 2041 to 2070 is also modelled in the DK-HIP model, however, precipitation increases most severely in the far future period (Pasten-Zapata et al., 2019), which makes far future more relevant to study with respect to landslide impacts. The WTD seasonality, i.e., amplitude representing the difference between dry summer and wet winter, was calculated based on the 10 m summer and winter WTD maps.

### 2.5 Precipitation data

We use precipitation data as an auxiliary variable in the analysis to investigate linkages between precipitation and landslide movement (step 2 in Fig. 3). The data originates from the 10 km by 10 km gridded precipitation dataset from the Danish Meteorological Institute (DMI) (Scharling, 1999). Data was extracted for a single 10 km grid cell which fully encompasses the study site. Data are available via DMI's free data API (DMI Weather archive Vejle, 2024). For the analysis we aggregated the daily precipitation timeseries to weekly values using the sum function.

### 2.6 Correlation analysis

Correlation analysis between movement data of the three landslides, WTD and precipitation was carried out in the R software package (A language and environment for statistical computing, 2023). Spearman's rank correlation coefficient ($\rho$) was calculated to investigate the extent of correlation between the WTD and the weekly LOS

280 movement of each landslide. Positive LOS movement rates were considered outliers and removed before the analysis. Spearman's rank correlation assesses the monotonicity of the relation between two variables which we favoured over Pearson correlation because of the expected non-linearity between WTD and InSAR landslide movement.

**3 Results**
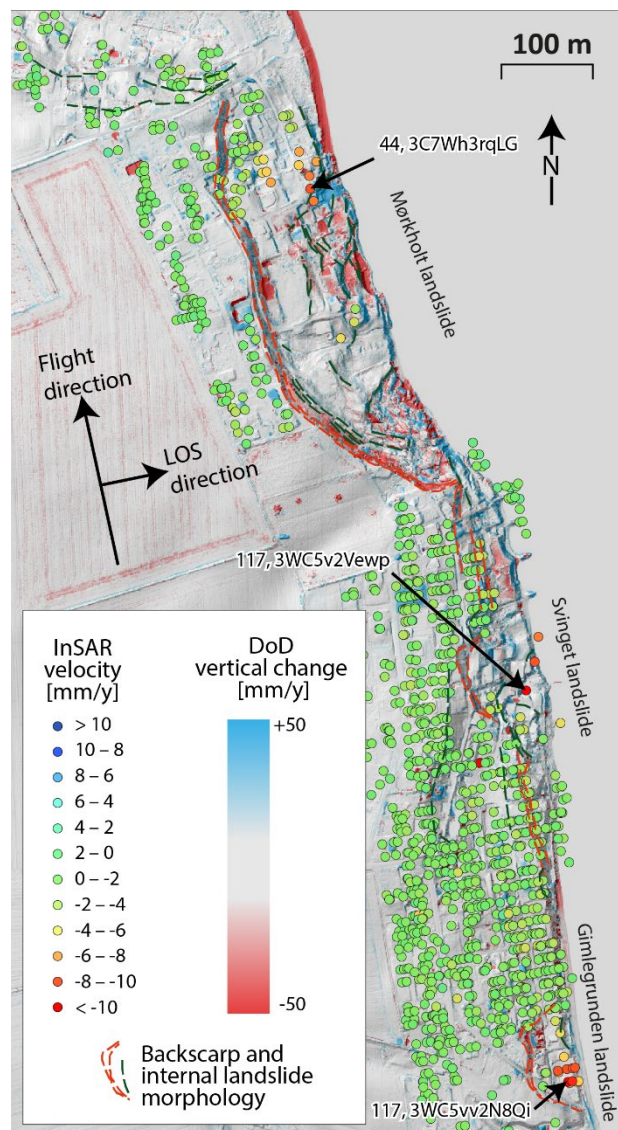
285

*Figure 3. [1 column] Landslide activity at the three landslides. DoD showing difference in elevation between 2014 and 2018 overlain with a hillshade model. InSAR points from tracks 44 and 117 are shown as points colored*

*according to their mean LOS velocities during 2015–2020. The numbered InSAR points marked with arrows refer to the timeseries shown in Fig. 6. The extent of the map is the same as Fig. 1c and d*

290

### 3.1 Spatial movement patterns of the landslides

For the Mørkholt landslide, the DoD shows subsidence along the backscarp and at the coast with a vertical component of up to 2.6 m over four years (equivalent to an average subsidence of 650 mm/y. InSAR reflectors are present in the northern part of the landslide, but are absent in the central and southern part where large DoD

295 anomalies are evident. The largest recorded InSAR movement is observed near the eastern row of houses with 5–10 mm/y. Field evidence of active deformation are ubiquitous across the landslide and include structural damage to fences and buildings, an open fracture with up to 30 cm vertical offset, an uplifted surface of black clay at the beach, rotated landslide blocks (Fig. 4), and springs (Fig. 1c, d).

300

*Figure 4 [1 column] a) Field photo of a large beech tree (Fagus sylvatica) on the Mørkholt landslide. The tree has been tilted by progressive landslide activity as shown by the upward changing dip of the trunk demonstrating the progressive and long-lived nature of the landslide. A minor scarp and the backscarp of the Mørkholt landslide are seen to the left of the tree. See Fig. 1d for location of photo. b) Photo taken in March 1981 at the head of the Svinget*

305 *landslide after a month of accelerated landslide activity. The photographer is standing on the southern part of the gravel road, the central part of which has subsided by 4–6 m over a month creating the present backscarp of the Svinget Landslide. See Fig. 1d for location of photo. Photo courtesy of Lars Hansen*

For the Svinget landslide, the DoD shows heterogenous movement across the landslide. Maximum average

310 subsidence of c. 70 mm/y are found in the northern part. Rotated landslide blocks bounded by steeper slopes of

around 40° inside the central and northern part of the landslide show a relative uplift in the DoD. The Svinget landslide has few  persistent scatter points in the central part of the landslide, close to the coast, with movement of up to 25 mm/y. InSAR points in the southern part of the landslide show no or little movement. Only few signs of active deformation were observed during June 2021 fieldwork, however, a brick-and-mortar house built across the backscarp in the northern part of the landslide was observed to be severely damaged. A local house owner explained that he re-levels his house every two to five years with a jack as landslide activity is tilting it, and that fractures appear in lawns and paths the same place every spring; near where InSAR data show highest movement rates (InSAR point ID "3WC5v2Vewp" in Fig. 3).

Historical records and information provided by local house owners informed us that the central part of the Svinget landslide had a period of rapid movement in the early 1980'ies mainly focused around February and March 1981. The landslide movement continued for a couple of years with one of the houses close to the backscarp moving by a total of 18 m, and 40 m of the road going through the landslide were damaged and had to be abandoned (Fig. 4b). Today this scarp is outlined by the 120 m wide slope centrally in the Svinget landslide. In association with this landslide activity, a coast parallel bar of clay emerged in the sea c. 30 m from the shore indicating that the seabed where the basal surface of rupture daylights was uplifted during the event. This feature was removed by wave erosion after some years, but a dark lineament on the seabed is still apparent in orthophotos (Fig. 1c). 1980 and 1981 were both extremely wet years with annual precipitation for both years being 100 mm above the Danish 1981–2010 normal (Cappelen, 2019). March of 1981 is the fourth wettest March on record in Denmark with total precipitation of 91 mm (Cappelen, 2019) .

The DoD does not show subsidence in the Gimlegrunden landslide. A DoD anomaly in the northern part of the landslide is probably due to excavation work. InSAR points are available throughout the landslide with movements of up to 10 mm/y. Movement is more pronounced near the coast. No clear signs of active deformation could be observed in the field.

**3.2 Temporal movement and dynamic conditioning factor pattern - InSAR movement and groundwater modelling results**

The average WTD seasonality expressed as the difference between long-term average winter and summer WTD (1991 - 2020), varied between circa 0 m and 2 m for the study site (Fig. 5). Fig. 6a depicts the average WTD seasonality over the three landslides for a five-year period. The dynamics are characterized by shallow groundwater levels during winter and deep groundwater levels during summer. Depending on precipitation and evapotranspiration during a year, the seasonality can vary between less than 1 m in 2017 to approximately 2 m in 2016 and 2018 (Fig. 6a). The highest WTD is simulated for the winters 2015/2016, 2017/18 and 2019/20 whereas the winters 2016/17 and 2018/19 have relatively deep normalized WTD. The WTD uncertainty for the study site also varies seasonally, with the highest variability found in months with the highest and lowest groundwater levels. More specifically the standard deviation can vary between approximately 0.1 m (December 2016) and 0.5 m (January 2016). Comparing the WTD seasonality shown in Fig. 5 and Fig. 6a underlines that a distinct variability in

space (Fig. 5) as well as in time (Fig. 6a) exists. The WTD timeseries shown in Fig. 6a is averaged over 16 simulation grids (shown in Fig. 5) and aggregated from daily to monthly timescale.
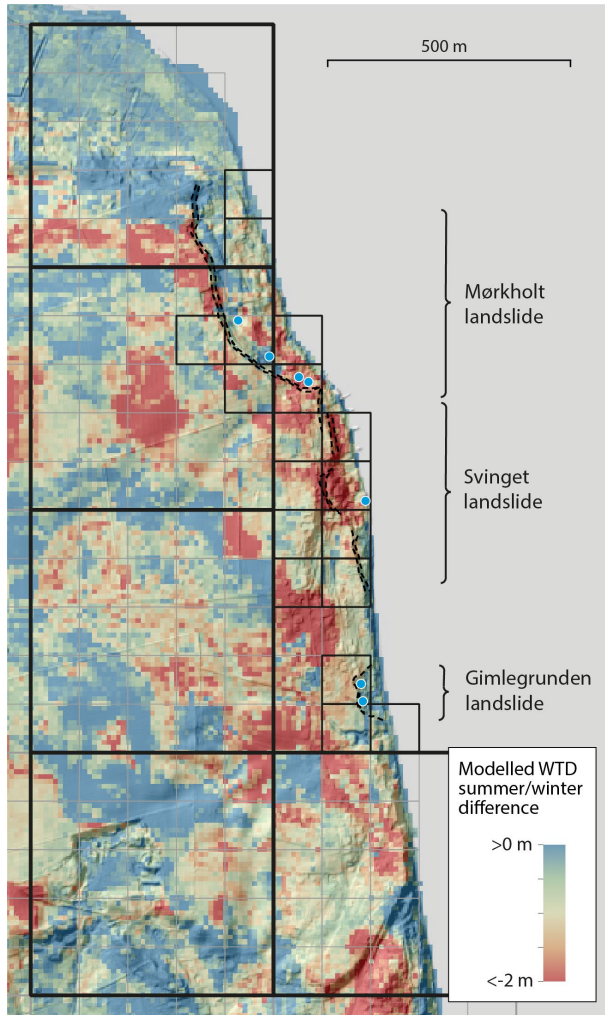
350 *Figure 5 [1 column] Danish Hydrology Information and Prognosis system (DK-HIP-model). Map showing the difference between the modelled summer and winter water table depth (WTD) in the study area for the period 1991 to 2020 downscaled following (Koch et al., 2021). The small 100 m grid cells highlighted in black (n=16) are used to calculate the WTD in Fig. 6a. Larger (500 m) grid cells (n=5) are used to analyse the climate change impact on WTD in Fig 7. The map is overlain by a hillshade. Mapped landslide backscarps are shown with black dashed lines.*

355 *Springs observed during fieldwork in June 2021 are indicated with blue dots. Note that the map extent is slightly larger than that in Fig. 1c and d to show the 500 m grid cells.*

Movement is observed exclusively in the winter seasons in the Mørkholt and Gimlegrunden landslides. For the Mørkholt landslide particularly large movements of 48 –72 mm/y are seen in the winters 2015/16, 2017/18 and

360 2019/20 (Fig. 6a). Our WTD time series does not include the entire 2019/20 season as the model only runs to December 2019. However, that winter was the wettest on record in Denmark. For the Svinget landslide, movement

occurs throughout the year but at various rates, with the fastest movement of up to 84 mm/y in winter and early spring (Fig. 6a).

The WTD shows a strong negative correlation (ρ ranges between -0.54 and -0.67) with movement for all three

365  landslides (Fig. 6b); when the water table is high, the weekly movement is also high and when the water table is low the weekly movement is also low. No correlation was found between the accumulated weekly precipitation and the InSAR movement of any of the three landslides.
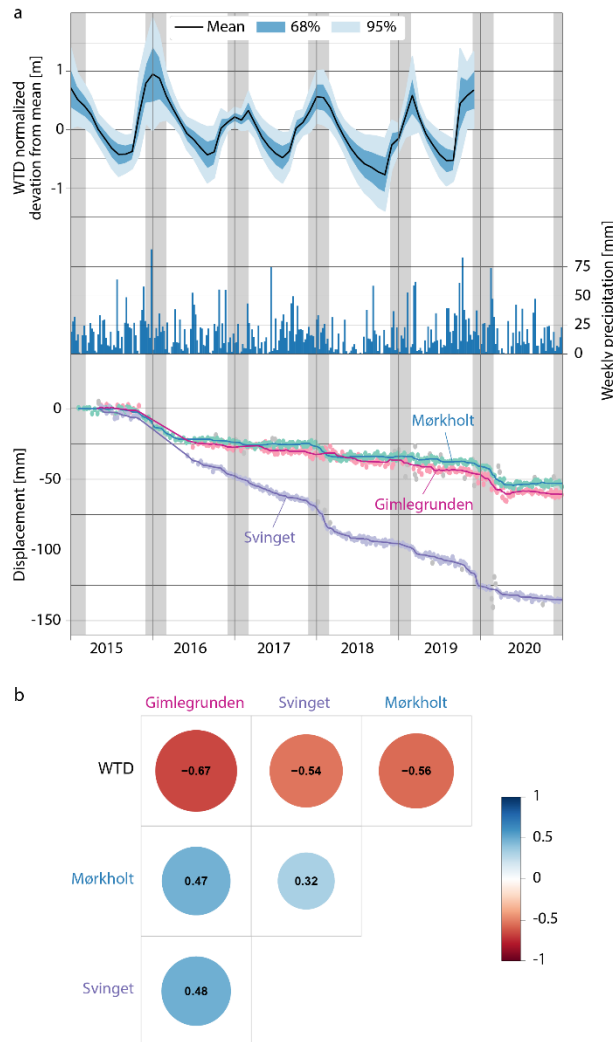
370  *Figure 6 [1 column]. a) Mean normalized WTD for the 16 selected 100 m grids (see Fig. 5) at monthly timescale and InSAR displacement data for three InSAR points within each landslide (see Fig. 3). Also shown is the weekly precipitation for the period. InSAR outliers disregarded for the running average calculation are coloured grey. Winter months (December, January, February) are shown as shaded grey bars to aid readability. b) Spearman's*

*rank correlation coefficient (ρ) derived from the WTD and the weekly movement for each of the three landslides.*

*Blue indicates positive and red negative correlations with p < 0.01.*

### 3.3 Climate modelling

To understand how climate change may impact future landslide activity, simulated groundwater levels for the study area were examined for the historic period 1990–2019 and for two climate scenarios RCP4.5 and RCP8.5 for the period 2071–2100. Fig. 7a depicts the long-term average and standard deviation of the historic WTD at monthly timescale for the 16 selected simulation grids shown in Fig. 5. The climate change impacts in Fig. 7b and c are averaged for the five 500 m simulation grids also shown in Fig. 5. WTD is expected to rise for all months towards end of the 21$^{st}$ century. The rise in WTD is more pronounced for RCP8.5 than for RCP4.5. The rise in WTD in the period 2071–2100 is most distinct during the winter months showing that we can expect wetter winters with a WTD in December up to 0.7 m higher relative to today following for the RCP8.5 (95% confidence interval) (red asterisk in Fig. 7c). The similar value for RCP4.5 (95% confidence interval) is 0.3 m (blue asterisk in Fig. 7b). These values are calculated by adding 2 * standard deviation to the mean.
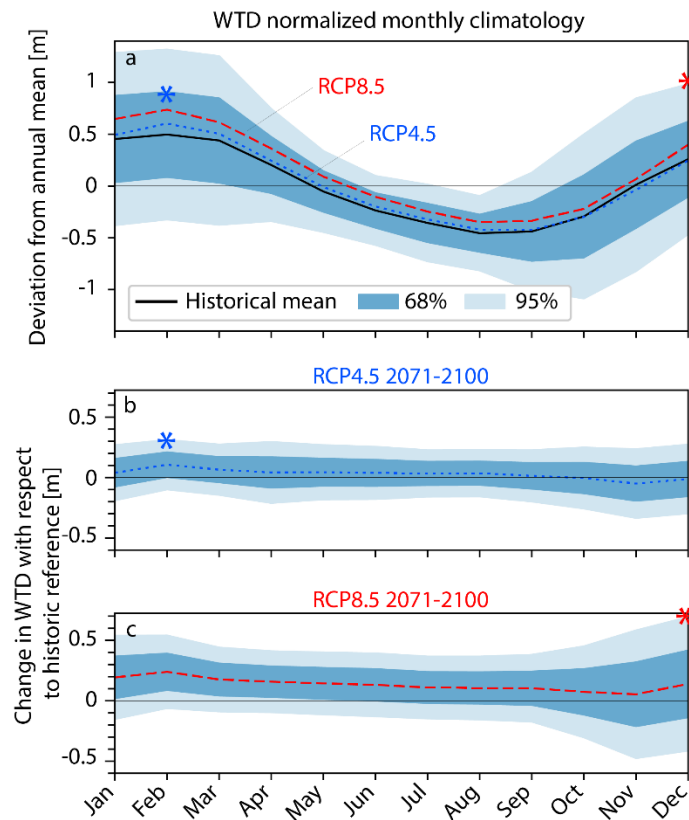
*Figure 7 [1 column]. Climate change scenarios. a) Monthly climatology for the historic period 1990–2019 for the normalized WTD 16 selected 100 m grids (Fig. 5). The mean +/- 68% and 95% confidence intervals are shown,*

*which represent the spatial variability across the study site. The red and blue asterisks indicate the maximum WTD values within RCP4.5 and 8.5 within 95% confidence interval, also shown in b and c. b) Simulated change in WTD for the period 2071–2100 based on RCP4.5 with respect to the historic reference. The blue asterisk is the maximum expected WTD of up to 0.3 m mentioned in the text using this RCP scenario. c) Simulated change in WTD for the period 2071–2100 based on RCP8.5 with respect to the historic reference. The red asterisk is the maximum expected WTD of up to 0.7 m mentioned in the text using this RCP scenario. The confidence intervals in b) and c) represent the variability origination from using an ensemble of climate models in the impact simulation. Dotted and dashed lines in b) and c) represent the ensemble mean and are added to the historic climatology in a).*

## 4 Discussion

### 4.1 WTD seasonality and landslide movement pattern

The observed landslide movement varies across and between seasons but is generally observed in the wet season (winter to early spring) with relatively shallow WTD (Fig. 6a). There is a clear correlation, for the whole timeseries examined, between WTD and landslide movement (Fig. 6b) whereas it is not possible to establish a correlation between weekly precipitation and landslide movement. This is because the dynamics in WTD are a result of multiple hydrological processes taking place, such as, precipitation, evapotranspiration, recharge and runoff, which are all accounted for in the DK-HIP model (Henriksen et al., 2020). The DK-HIP model is based on a coupled surface-subsurface hydrological model that integrates national databases of borehole information, geophysics and observations of river discharge and groundwater head. Our correlation analysis (Fig. 6b) shows that these processes need to be considered when studying landslide movement either by on site monitoring or, as in our case, by modelling and remote sensing. This is at least valid for the temperate climate conditions of Denmark where rainfall is often evenly distributed over the year (see fig. 6a) and WTD dynamics are modulated by the seasonality of air temperature and thereby potential evapotranspiration. Under different climate conditions, e.g., where precipitation has a more distinct seasonality the correlation between terrain movement and precipitation may be higher (Handwerger et al., 2022; Cohen-Waeber et al., 2018; Wistuba et al., 2021).

In relatively dry winter/early spring seasons of 2016/2017 and 2018/2019, where the normalized WTD is generally below +0.5 m, seasonal movement is not observed for the three landslides. In the winter seasons of 2015/16, 2017/18 and 2019/20 the mean normalized WTD exceeded c. +0.5 m and landslide movement is observed. We thus estimate an empirical threshold for landslide movement for the three landslides is at c. +0.5 m normalized WTD. A more detailed investigation, preferable with in-situ measurements would be required to properly constrain a critical WTD threshold for seasonal landslide movement.

### 4.2 Climate projections and landslide evolution

We can quantify an overall increase in mean WTD by 2071–2100 for both RCP4.5 and RCP8.5 (Figs. 7b, c). For RCP8.5, the increase in WTD is predicted to be up to 0.7 m (95 % confidence interval), mainly focussed in the

winter season (red asterisk in Fig. 7c). This trend will lead to wetter initial conditions meaning that less precipitation in an event will be required to achieve critical WTD levels and increased weight of the landslide body leading to decrease of the basal shear strength (Crozier, 2010). This will overall lead to increased seasonal landslide activity.

430     If 0.7 m of WTD increase is applied to the dry seasons of 2016/17 and 2018/19, where normalized WTD in the winter season under current conditions does not exceed +0.5 m, then the landslides would experience a WTD similar to the one evident for the seasons 2015/16, 2017/18 and 2019/20 that are some of the wettest seasons (by precipitation) on record in Denmark to date (Cappelen, 2019).

The wet seasons of 2015/16, 2017/18 and 2019/20, exhibiting a normalized WTD above +0.5 m, would with
435     increase in WTD of 0.7 m experience values that fall beyond the 95% confidence interval in Fig. 7a (red asterisk). WTD would thus exceed what this area has likely experienced in the modelled historical period 1990–2019.

The wet seasons of 2015/16, 2017/18, and 2019/20, with a normalized WTD greater than +0.5 m, would result in an elevated WTD of 0.7 m, exceeding the 2-standard deviation interval depicted in Fig. 7a (represented by a red asterisk) and surpassing historical modelled values from the period 1990–2019.

440     RCP4.5 predicts up to 0.3 m increase in normalized WTD in the winters at the end of this century (95 % confidence interval, Fig. 7b). This will potentially elevate WTD of dry winters such as 2016/17 and 2018/19 up to above the +0.5 m threshold making them wetter than average WTD for the historic period (Fig. 7a). In wet years such as 2015/16, 2017/18 and 2019/20, WTD will potentially increase to within the 95% confidence interval of historic WTD levels (Fig. 7a) also surpassing most modelled historical WTD levels. Thus, the RCP4.5 scenario also points
445     towards increasing landslide activity and likelihood of thresholds being breached.

The response of the landslides to such a potential breach of thresholds may be similar to the historical case of extreme sliding that occurred in the Svinget landslide in 1981. Here individual houses moved by 18 m over a year mainly focused on February and March (>1500 mm/month average over the year) leading to structural damages on roads and buildings. This occurred during the, at that time, wettest winter in Denmark only to be surpassed in recent
450     decades (Cappelen, 2019). This demonstrates that these landslides can accelerate from slow to moderate velocities warranting evacuation (*sensu* (Hungr et al., 2014) during extreme events, which we show are likely to increase in frequency. This is however a hypothetical conclusion without knowing the WTD at the time of this historic landslide activity.

Other dynamic conditioning factors for landslide movement such as increased coastal erosion caused by higher sea
455     level and storm wave activity along with a projected increase in extreme rainfall events (Crozier, 2010) are not included in our present analysis. However, these are also projected to change (DMI Klimaatlas, 2023) in a direction that is expected to accelerate landslide movement. Thus, all the main natural dynamic conditioning factors controlling landslide activity are shifting towards increasing landslide activity. In an area with many similar landslides of low activity such as Denmark (Herrera et al., 2018; Mateos et al., 2020; Svennevig et al., 2020) the net
460     result is likely to be an increased landslide activity both as an increase in landslide movement as well as potential expansion of currently active landslides and development of new coastal landslides. This will pose new challenges

to authorities, landowners and decision makers that have little or no experience in dealing with the consequences of landslides.

The impact of climate change on landslides has been investigated in several studies, with varying results. For example, (Dixon and Brook, 2007) found that the instability threshold of examined landslides could decrease under the medium-high climate change scenario, while (Collison et al., 2000) found no significant change in the frequency of large landslides in SE England due to the projected increased rainfall being matched by increases in evapotranspiration. In contrast, (Lin et al., 2022) discovered that the extent of landslide-susceptible terrain and the frequency of landslide-triggering rainfall will increase under climate change in China, but noted a spatially heterogeneous pattern.(Peres and Cancelliere, 2018) found a general tendency for a decrease in landslide hazard due to progressive climate change in a site in Italy. The differing outcomes of these and other studies along with our present contribution highlight the site and region-specific impacts of climate change on landslides.

**4.3 Limitations and benefits of using free and publicly available data**

The empirical threshold of +0.5 m WTD for landslide activation is not universal and can vary depending on site-specific factors, such as topography, geology, and climate. However, the workflow outlined in Fig. 2 can be applied widely as larger datasets on dynamic conditioning become available. Our study is based on a limited dataset, and longer time periods would increase the robustness of our correlation analysis. InSAR data from EGMS are freely available for all of Europe, with periodic updates planned to provide longer movement time series for analysis. Furthermore, the WTD model used here is planned to be rerun up to the present and future predictions refined, which will no doubt nuance our current findings.

Although this workflow based solely on remotely sensed and modelling data (Fig. 2) is not a substitute for on-site monitoring, it can serve as an initial screening process to inexpensively screen landslides for sensitivity to projected climate change in areas where remote data on dynamic conditioning factors along with movement data are available. This information can help prioritize resources for further investigations and monitoring. However, in-depth studies on landslides, e.g., linking WTD and landslide movement, should preferably use local groundwater models calibrated with in situ measurements, as they can better incorporate local hydrogeology. Moreover, the DK-HIP-model was calibrated to average WTD conditions, so we recommend that local groundwater models be calibrated to better represent extreme wet conditions, with a focus on the effects of high-intensity precipitation events on WTD, as landslide movement is sensitive to extreme WTD.

When it comes to transferring our approach to other case studies more limitations may arise. These may be due to data variable data availability and quality. Namely the availability of high quality DEM's and sufficient quality data on dynamic preconditioning factors. Site specific InSAR limitations regarding geometry and LOS issues, vegetation, snow-cover, displacement rates exceeding wavelength associated thresholds should also be considered.

Integrating DoD and InSAR PS datasets has a huge potential and the two methods are highly supplementary. DoD anomalies are confident in areas where there are no natural InSAR reflectors and where LOS displacement rates

exceed wavelength associated thresholds. At Mørkholt only houses moving by less than c. 100 mm/y provide good InSAR reflectors. By integrating the two datasets, as demonstrated here, we can infer PS time series to represent movement in a landslide area outlined by a DoD anomaly. Similarly, deformation rates (LOS for PS and vertical subsidence for DOD) can be compared and discussed against each other. However it should be stressed that these numbers do not represent the same direction and time resolution.

**5 Conclusions**

Seasonal activity in three large slow-moving coastal landslides in Denmark correlates with modelled changes in water table depth (WTD). When normalized WTD exceeds +0.5 m in the winter season in wet years seasonal movement commences. Weekly precipitation data shows no correlation with landslide movement.

WTD is projected to increase by up to 0.7 m towards 2100 AD (RCP8.5, 95% confidence interval) in this area. These WTD values exceed what this area has experienced in the past decades (1990–2019) and this is likely to result in increasing landslide activity as the landslides equilibrates to the changing conditions. The RCP4.5 scenario also points to increased activity in the landslides.

A historic case from 1981 of accelerated landslide movement resulting in serious structural damage may serve as an example of an extreme event we will see more of in the future as a direct result of elevated WTD caused by climate change.

Our study highlights the potential of utilizing high-quality publicly available data to address complex scientific questions and presents a workflow for doing this. The quality and quantity of such data is ever increasing and so is the potential of such approach.

**Competing interests**

The authors declare that they have no conflict of interest.

**Data availability**

All data is publicly available from the links in section 2: Data and methods.

**Funding**

Field validation of the remotely sensed observations was conducted within a project financed by Vejle Municipality. GL has received funding from the European Union's Horizon 2020 research and innovation program under the Marie Skłodowska-Curie grant agreement No 801199.

**Acknowledgement**

Residents of Mørkholt are thanked for their cooperation. Lars Hansen is thanked for information on the 1981 event

530    and the use of photos he took during the event (Fig. 4b). Vejle Municipality is thanked for cooperation during

fieldwork and aid in communication with local stakeholders. Two anonymous reviewers are thanked for their

reviews.

**CRediT authorship contribution statement**

535    Kristian Svennevig: Conceptualization; Data curation; Formal synthesis analysis; Writing – original draft and

Review & Editing. Julian Koch: Formal analysis of the DK-HIP-model; Writing - Review & Editing. Marie

Keiding: Formal analysis of InSAR; Writing - Review & Editing. Gregor Luetzenburg: Formal analysis of DoD and

correlation analysis; Writing - Review & Editing.

540    **References**

Abbott, M. B., Bathurst, J. C., Cunge, J. A., O'Connell, P. E., and Rasmussen, J.: An introduction to the European Hydrological System — Systeme Hydrologique Europeen, "SHE", 1: History and philosophy of a physically-based, distributed modelling system, Journal of Hydrology, 87, 45–59, 1986.

Alberti, S., Olsen, M. J., Allan, J., and Leshchinsky, B.: Feedback thresholds between coastal retreat and
545    landslide activity, Engineering Geology, 106620, https://doi.org/10.1016/j.enggeo.2022.106620, 2022.

DMI Weather archive Vejle: https://www.dmi.dk/lokationarkiv/show/DK/2621215/Greve?cHash=cd7318c15ef5cd901a6038c352a7d4ed, last access: 25 January 2024.

European Ground Motion Service — Copernicus Land Monitoring Service:
550    https://land.copernicus.eu/en/products/european-ground-motion-service, last access: 29 January 2024.

Hydrologisk Informations- og Prognosesystem: https://hip.dataforsyningen.dk/, last access: 29 January 2024.

Jupiter database drill log: https://data.geus.dk/JupiterWWW/borerapport.jsp?borid=458263, last access: 13 December 2023.

555    van Asch, T. W. J. and Buma, J. T.: Modelling groundwater fluctuations and the frequency of movement of a landslide in the Terres Noires region of Barcelonnette (France), Earth Surface Processes and Landforms, 22, 131–141, https://doi.org/10.1002/(SICI)1096-9837(199702)22:2<131::AID-ESP679>3.0.CO;2-J, 1997.

van Asch, T. W. J., Buma, J., and Van Beek, L. P. H.: A view on some hydrological triggering systems in
560    landslides, Geomorphology, 30, 25–32, https://doi.org/10.1016/S0169-555X(99)00042-2, 1999.

van Asch, T. W. J., Malet, J. P., and Bogaard, T. A.: The effect of groundwater fluctuations on the velocity pattern of slow-moving landslides, Natural Hazards and Earth System Science, 9, 739–749, https://doi.org/10.5194/nhess-9-739-2009, 2009.

565    Bennett, G. L., Roering, J. J., Mackey, B. H., Handwerger, A. L., Schmidt, D. A., and Guillod, B. P.: Historic drought puts the brakes on earthflows in Northern California, Geophysical Research Letters, 43, 5725–5731, https://doi.org/doi:10.1002/ 2016GL068378, 2016.

Cappelen, J.: Ekstrem nedbør i Danmark - opgørelser og analyser til og med 2018, Danmarks Meteorologiske Institut, Copenhagen, 2019.

Coe, J. A.: Regional moisture balance control of landslide motion: Implications for landslide forecasting
570    in a changing climate, Geology, 40, 323–326, https://doi.org/10.1130/G32897.1, 2012.

Coe, J. A., Michael, J. A., Crovelli, R. A., Savage, W. Z., Laprade, W. T., and Nashem, W. D.: Probabilistic assessment of precipitation-triggered landslides using historical records of landslide occurence, Seattle, Washington, Environmental and Engineering Geoscience, 10, 103–122, https://doi.org/10.2113/10.2.103, 2004.

575    Cohen-Waeber, J., Bürgmann, R., Chaussard, E., Giannico, C., and Ferretti, A.: Spatiotemporal Patterns of Precipitation-Modulated Landslide Deformation From Independent Component Analysis of InSAR Time Series, Geophysical Research Letters, 45, 1878–1887, https://doi.org/10.1002/2017GL075950, 2018.

Collison, A., Wade, S., Gri, J., and Dehn, M.: Modelling the impact of predicted climate change on landslide frequency and magnitude in SE England, Engenering Geology, 55, 205–218, 2000.

580    Corominas, J., Moya, J., Ledesma, A., Lloret, A., and Gili, J. A.: Prediction of ground displacements and velocities from groundwater level changes at the Vallcebre landslide (Eastern Pyrenees, Spain), Landslides, 2, 83–96, https://doi.org/10.1007/s10346-005-0049-1, 2005.

Costantini, M., Minati, F., Trillo, F., Ferretti, A., Passera, E., Rucci, A., Dehls, J., Larsen, Y., Marinkovic, P., Eineder, M., Brcic, R., Siegmund, R., Kotzerke, P., Kenyeres, A., Costantini, V., Proietti, S., Solari, L., and
585    Andersen, H. S.: EGMS: Europe-Wide Ground Motion Monitoring based on Full Resolution Insar Processing of All Sentinel-1 Acquisitions, in: IGARSS 2022 - 2022 IEEE International Geoscience and Remote Sensing Symposium, Citation Key: 9884966, 5093–5096, https://doi.org/10.1109/IGARSS46834.2022.9884966, 2022.

Crosetto, M., Monserrat, O., Cuevas-González, M., Devanthéry, N., and Crippa, B.: Persistent Scatterer
590    Interferometry: A review, ISPRS Journal of Photogrammetry and Remote Sensing, 115, 78–89, https://doi.org/10.1016/j.isprsjprs.2015.10.01, 2016.

Crosetto, M., Solari, L., Mróz, M., Balasis-Levinsen, J., Casagli, N., Frei, M., Oyen, A., Moldestad, D. A., Bateson, L., Guerrieri, L., Comerci, V., and Andersen, H. S.: The evolution of wide-area DInSAR: From regional and national services to the European ground motion service, Remote Sensing, 12, 1–20,
595    https://doi.org/10.3390/RS12122043, 2020.

Crozier, M. J.: Deciphering the effect of climate change on landslide activity: A review, Geomorphology, 124, 260–267, https://doi.org/10.1016/j.geomorph.2010.04.009, 2010.

Dixon, N. and Brook, E.: Impact of predicted climate change on landslide reactivation: Case study of Mam Tor, UK, Landslides, 4, 137–147, https://doi.org/10.1007/s10346-006-0071-y, 2007.

600     DMI Klimaatlas: https://www.dmi.dk/klima-atlas/data-i-klimaatlas/, last access: 30 January 2023.

Ferretti, A., Prati, C., and Rocca, F.: Permanent Scatterers in SAR Interferometry, IEEE Transactions on Geoscience and Remote Sensing, 39, 8–20, 2001.

Froude, M. J. and Petley, D. N.: Global fatal landslide occurrence from 2004 to 2016, Natural Hazards and Earth System Sciences, 18, 2161–2181, https://doi.org/10.5194/nhess-18-2161-2018, 2018.

605     Gariano, S. L. and Guzzetti, F.: Landslides in a changing climate, Earth-Science Reviews, 162, 227–252, https://doi.org/10.1016/j.earscirev.2016.08.011, 2016.

Håkansson, E. and Pedersen, S. A. S.: Geologisk Kort over den Danske Undergrund, Varv, 1992.

Handwerger, A. L., Fielding, E. J., Huang, M. H., Bennett, G. L., Liang, C., and Schulz, W. H.: Widespread Initiation, Reactivation, and Acceleration of Landslides in the Northern California Coast Ranges due to
610     Extreme Rainfall, Journal of Geophysical Research: Earth Surface, 124, 1782–1797, https://doi.org/10.1029/2019JF005035, 2019.

Handwerger, A. L., Fielding, E. J., Sangha, S. S., and Bekaert, D. P. S.: Landslide Sensitivity and Response to Precipitation Changes in Wet and Dry Climates, Geophysical Research Letters, 49, 1–12, https://doi.org/10.1029/2022GL099499, 2022.

615     Heilmann-Clausen, C., Nielsen, O. B., and Gersner, F.: Lithostratigraphy and depositional environments in the Upper Paleocene and Eocene of Denmark, Bulletin of the Geological Society of Denmark, 33, 287–323, 1985.

Henriksen, H. J., Troldborg, L., Nyegaard, P., Sonnenborg, T. O., Refsgaard, J. C., and Madsen, B.: Methodology for construction, calibration and validation of a national hydrological model for Denmark,
620     Journal of Hydrology, 280, 52–71, 2003.

Henriksen, H. J., Kragh, S. J., Gotfredsen, J., Ondracek, M., van Til, M., Jakobsen, A., Schneider, R. J. M., Koch, J., Troldborg, L., Rasmussen, P., Pasten-Zapata, E., and Stisen, S.: Dokumentationsrapport vedr. modelleverancer til Hydrologisk Informations- og Prognosesystem, 2020.

Hermanns, R. L., Niedermann, S., Villanueva Garcia, A., and Schellenberger, A.: Rock avalanching in the
625     NW argentine andes as a result of complex interactions of lithologic, structural and topographic boundary conditions, climate change and active tectonics, in: Landslides from Massive Rock Slope Failure, edited by: Evans, S. G., Scarawcia Mugnozza, G., Strom, A. L., and Hermanns, R. L., Springer Netherlands, Celano, 497–520, 2006.

Herrera, G., Mateos, R. M., García-Davalillo, J. C., Grandjean, G., Poyiadji, E., Maftei, R., Filipciuc, T. C.,
630     Jemec Auflič, M., Jež, J., Podolszki, L., Trigila, A., Iadanza, C., Raetzo, H., Kociu, A., Przyłucka, M., Kułak, M., Sheehy, M., Pellicer, X. M., McKeown, C., Ryan, G., Kopačková, V., Frei, M., Kuhn, D., Hermanns, R. L., Koulermou, N., Smith, C. A., Engdahl, M., Buxó, P., Gonzalez, M., Dashwood, C., Reeves, H., Cigna, F., Lik, P., Pauditš, P., Mikulėnas, V., Demir, V., Raha, M., Quental, L., Sandić, C., Fusi, B., and Jensen, O. A.:

Landslide databases in the Geological Surveys of Europe, Landslides, 15, 359–379, https://doi.org/10.1007/s10346-017-0902-z, 2018.

635

Højberg, A. L., Troldborg, L., Stisen, S., Christensen, B. B., and Henriksen, H. J.: Stakeholder driven update and improvement of a national water resources model, Environmental modelling & software, 40, 202–213, 2013.

Hungr, O., Leroueil, S., and Picarelli, L.: The Varnes classification of landslide types, an update,

640    Landslides, 11, 167–194, https://doi.org/10.1007/s10346-013-0436-y, 2014.

Iverson, R. M.: Landslide triggering by rain infiltration, Water Resources Research, 36, 1897–1910, https://doi.org/10.1029/2000WR900090, 2000.

Kashyap, R., Pandey, A. C., and Parida, B. R.: Spatio-temporal variability of monsoon precipitation and their effect on precipitation triggered landslides in relation to relief in Himalayas, Spatial Information

645    Research, 29, 857–869, https://doi.org/10.1007/s41324-021-00392-8, 2021.

Koch, J., Gotfredsen, J., Schneider, R., Troldborg, L., Stisen, S., and Henriksen, H. J.: High resolution water table modelling of the shallow groundwater using a knowledge-guided gradient boosting decision tree model, Frontiers in Water, 3, https://doi.org/DOI=10.3389/frwa.2021.701726, 2021.

Lin, Q., Steger, S., Pittore, M., Zhang, J., Wang, L., Jiang, T., and Wang, Y.: Evaluation of potential changes

650    in landslide susceptibility and landslide occurrence frequency in China under climate change, Science of the Total Environment, 850, 158049, https://doi.org/10.1016/j.scitotenv.2022.158049, 2022.

Luetzenburg, G., Svennevig, K., Bjørk, A. A., Keiding, M., and Kroon, A.: A national landslide inventory of Denmark, Earth System Science Data, 2022, 1–13, 2022.

Luna, L. V. and Korup, O.: Seasonal Landslide Activity Lags Annual Precipitation Pattern in the Pacific

655    Northwest, Geophysical Research Letters, 49, 1–11, https://doi.org/10.1029/2022gl098506, 2022.

Magnin, F., Josnin, J. Y., Ravanel, L., Pergaud, J., Pohl, B., and Deline, P.: Modelling rock wall permafrost degradation in the Mont Blanc massif from the LIA to the end of the 21st century, Cryosphere, 11, 1813–1834, https://doi.org/10.5194/tc-11-1813-2017, 2017.

Magnin, F., Etzelmüller, B., Westermann, S., Isaksen, K., Hilger, P., and Hermanns, R. L.: Permafrost

660    distribution in steep rock slopes in Norway : measurements , statistical modelling and implications for geomorphological processes, Earth Surface Dynamics, 7, 1019–1040, 2019.

Malet, J.-P., van Asch, T. W. J., van Beek, R., and Maquaire, O.: Forecasting the behaviour of complex landslides with a spatially distributed hydrological model, Natural Hazards and Earth System Sciences, 5, 71–85, https://doi.org/10.5194/nhess-5-71-2005, 2005.

665    Mateos, R. M., López-Vinielles, J., Poyiadji, E., Tsagkas, D., Sheehy, M., Hadjicharalambous, K., Liscák, P., Podolski, L., Laskowicz, I., Iadanza, C., Gauert, C., Todorović, S., Auflič, M. J., Maftei, R., Hermanns, R. L., Kociu, A., Sandić, C., Mauter, R., Sarro, R., Béjar, M., and Herrera, G.: Integration of landslide hazard into urban planning across Europe, Landscape and Urban Planning, 196, https://doi.org/10.1016/j.landurbplan.2019.103740, 2020.

670 Moreiras, S., Lisboa, M. S., and Mastrantonio, L.: The role of snow melting upon landslides in the central Argentinean Andes, Earth Surface Processes and Landforms, 37, 1106–1119, https://doi.org/10.1002/esp.3239, 2012.

Nuth, C. and Kääb: Co-registration and bias corrections of satellite elevation data sets for quantifying glacier thickness change, Cryosphere, 5, 271–290, https://doi.org/10.5194/tc-5-271-2011, 2011.

675 Pasten-Zapata, E., Sonnenborg, T. O., and Refsgaard, J. C.: Climate change: Sources of uncertainty in precipitation and temperature projections for Denmark, GEUS Bulletin, 43, https://doi.org/10.34194/GEUSB-201943-01-02, 2019.

Penna, I. M., Magnin, F., Nicolet, P., Etzelmüller, B., Hermanns, R. L., Böhme, M., Kristensen, L., Nöel, F., Bredal, M., and Dehls, J. F.: Permafrost controls the displacement rates of large unstable rock-slopes in 680 subarctic environments, Global and Planetary Change, 220, https://doi.org/10.1016/j.gloplacha.2022.104017, 2023.

Peres, D. J. and Cancelliere, A.: Modeling impacts of climate change on return period of landslide triggering, Journal of Hydrology, 567, 420–434, https://doi.org/10.1016/j.jhydrol.2018.10.036, 2018.

Pfeiffer, J., Zieher, T., Bremer, M., Wichmann, V., and Rutzinger, M.: Derivation of Three-Dimensional 685 Displacement Vectors from Multi-Temporal Long-Range Terrestrial Laser Scanning at the Reissenschuh Landslide (Tyrol, Austria), Remote Sensing, 10, 1688, https://doi.org/10.3390/rs10111688, 2018.

Pollock, W. and Wartman, J.: Human Vulnerability to Landslides, GeoHealth, 4, 1–17, https://doi.org/10.1029/2020GH000287, 2020.

Rasmussen, E. S., Dybkjær, K., and Piasecki, S.: Lithostratigraphy of the Upper Oligocene – Miocene 690 succession of Denmark, Geological Survey of Denmark and Greenland Bulletin, 22, 92 pp., 2010.

A language and environment for statistical computing: https://www.r-project.org/, last access: 30 January 2023.

Rosen, P. A., Hensley, S., Joughin, I. R., Li, F. K., Madsen, S. N., Rodriguez, E., and Goldstein, R.: Synthetic aperture radar interferometry, Proc. of the IEEE, 88, 333–382, https://doi.org/10.1109/5.838084, 2000.

695 Saba, S. B., van der Meijde, M., and van der Werff, H.: Spatiotemporal landslide detection for the 2005 Kashmir earthquake region, Geomorphology, 124, 17–25, https://doi.org/10.1016/j.geomorph.2010.07.026, 2010.

Scaioni, M., Longoni, L., Melillo, V., and Papini, M.: Remote Sensing for Landslide Investigations: An Overview of Recent Achievements and Perspectives, Remote Sensing, 6, 700 https://doi.org/doi:10.3390/rs60x000x, 2014.

Scharling, M.: Klimagrid Danmark Nedbør 10x10 km (ver. 2) - Metodebeskrivelse, Danish Meteorological Institute Technical Report, Danish Meteorological Institute, Copenhagen, 1999.

SDFI: Denmark's Elevation Model, 2020.

Svennevig, K. and Keiding, M.: En dansk nomenklatur for landskred, Geologisk Tidsskrift, 2020, 19–30, 2020.

Svennevig, K., Luetzenburg, G., Keiding, M. K., Pedersen, S. A. S., Asbjørn, S., and Pedersen, S. A. S.: Preliminary landslide mapping in Denmark indicates an underestimated geohazard, GEUS Bulletin, 44, 1–6, https://doi.org/10.34194/geusb.v44.5302, 2020.

Svennevig, K., Hermanns, R. L., Keiding, M., Binder, D., Citterio, M., Dahl-Jensen, T., Mertl, S., Sørensen, E. V., and Voss, P. H.: A large frozen debris avalanche entraining warming permafrost ground—the June 2021 Assapaat landslide, West Greenland, Landslides, https://doi.org/10.1007/s10346-022-01922-7, 2022.

Svennevig, K., Keiding, M., Korsgaard, N. J., Lucas, A., Owen, M., Poulsen, M. D., Priebe, J., Sørensen, E. V., and Morino, C.: Uncovering a 70-year-old permafrost degradation induced disaster in the Arctic, the 1952 Niiortuut landslide-tsunami in central West Greenland, Science of The Total Environment, 859, 160110, https://doi.org/10.1016/j.scitotenv.2022.160110, 2023.

Terzaghi, K.: Mechanism of Landslides, edited by: Paige, S., Geological Society of America, 0 pp., https://doi.org/10.1130/Berkey.1950.83, 1950.

Uhlemann, S., Smith, A., Chambers, J., Dixon, N., Dijkstra, T., Haslam, E., Meldrum, P., Merritt, A., Gunn, D., and Mackay, J.: Assessment of ground-based monitoring techniques applied to landslide investigations, Geomorphology, 253, 438–451, https://doi.org/10.1016/j.geomorph.2015.10.027, 2016.

Van Beek, L. P. H. and Van Asch, T. W. J.: Regional assessment of the effects of land-use change on landslide hazard by means of physically based modelling, Natural Hazards, 31, 289–304, https://doi.org/10.1023/B:NHAZ.0000020267.39691.39, 2004.

Vitousek, S., Buscombe, D., Vos, K., Barnard, P. L., Ritchie, A. C., and Warrick, J. A.: The future of coastal monitoring through satellite remote sensing, Cambridge Prisms: Coastal Futures, 1, https://doi.org/10.1017/cft.2022.4, 2023.

Wistuba, M., Gorczyca, E., and Malik, I.: Inferring precipitation thresholds of landslide activity from long-term dendrochronological and precipitation data: Case study on the unstable slope at Karpenciny, Poland, Engineering Geology, 294, 18, https://doi.org/10.1016/j.enggeo.2021.106398, 2021.

Zieher, T., Gallotti, G., Rianna, G., Reder, A., and Pfeiffer, J.: Exploring the effects of climate change on the water balance of a continuously moving deep-seated landslide, Nat Hazards, 115, 357–387, https://doi.org/10.1007/s11069-022-05558-7, 2023.